Optical chromatic confocal probes

H.-J.Jordan
DIGITAL SURF Deutschland GmbH, Weinbrennerstasse 4,
D-77815 Bühl, Germany
Phone +49 (0)7223 9539300, Fax +49 (0)7223 9539306
www.digitalsurf.de, contact@digitalsurf.de

Abstract: There is a growing need in many industrial applications to replace contact measurement instruments by suitable non-contact techniques, either due to a demand of higher measurement speed or due to touch sensitive surfaces. The optical technique of (single point) chromatic confocal probes seems to turn out as the industry's favourite candidate for such non-contact applications with function-relevant characterisation, as these purely passive optical probes are scalable in a distance measurement range from microns to centimetres with high resolution in distance as well as lateral. Thus, roughness / surface texture as well as contour measurements can be done using the same optical measurement principle.

1. THE BASIC PRINCIPLE OF CONFOCAL DISTANCE MEASUREMENT

The principle of monochromatic confocal distance measurement is shown in Figure 1 [Minsky 1957, Minsky 1988]. A diffraction limited illumination lens images the light as emitted from a point light source into a perfect focus of highest illumination density (first focusing = illumination). If the surface distance to be measured is exactly "in focus", the focused surface is imaged by a diffraction limited imaging lens onto a point detector, which detects an intensity maximum (second focusing = imaging with the highest flux of light through a detector pinhole in front of an extended detector). This can happen either in transmission as well as in reflection mode. In reflection mode, the same diffraction limited optics will be passed twice. Thus, this principle is also called "distance measurement by double focusing" (upper half of Figure 1).

If the surface distance is defocused (lower half of Figure 1), then the flux of light through the detector pinhole is reduced by two effects. First, the surface is illuminated with a reduced density due to the defocusing in illumination. Second, the surface is also defocused with respect to the detector, which results in another reduction of the light density in front of the detector pinhole. As a result, the point detector detects an intensity which is rapidly decreasing with the degree of the defocused z-coordinate and which is Gaussian-shaped. This so called "depth discrimination" effect [Hamilton 1981, Wilson 1989, Wilson 1990] allows an accurate determination of the distance to be measured by analysing a z-scan of the intensity depth response.

Another advantage of this measurement principle is the suppression of stray-light from defocused object regions, which results in contrast enhancement. An additional synchronized xy-scan of both the point light source as well as the point detector results in 3D-topography measurement. Various technical designs have successfully been used for the 3D-characterisation of technical surfaces [Petran 1968, Hamilton 1982, Carlsson 1987, Jordan 1997, Jordan 1998, Jordan 2000, Jordan 2001].

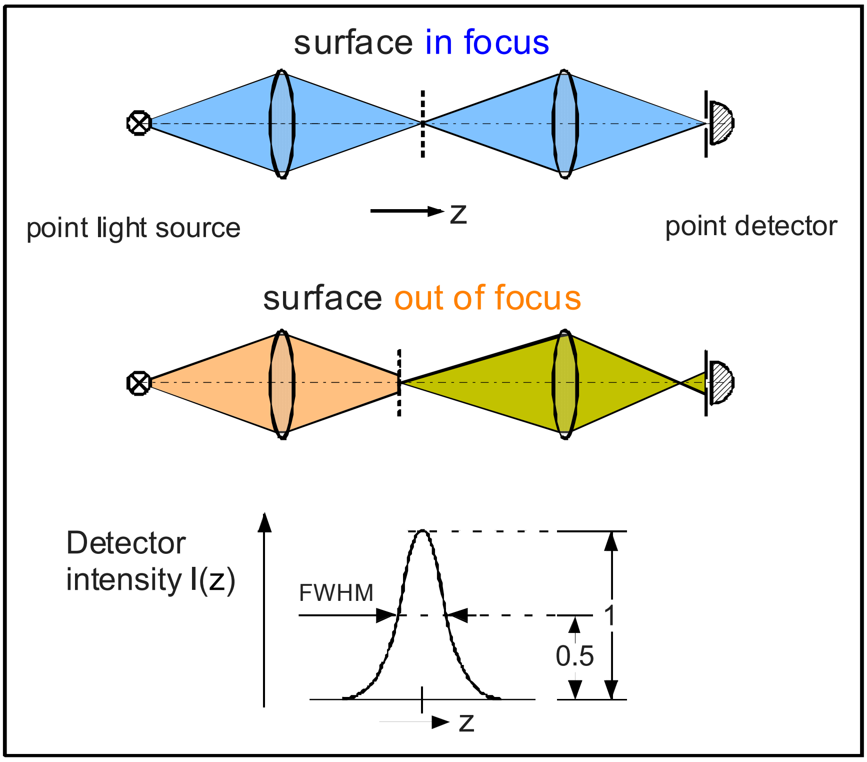

Figure 1: Basic principle of monochromatic confocal distance measurement.

2. THE PRINCIPLE OF CHROMATIC CONFOCAL DISTANCE PROBES

In monochromatic or axially colour corrected confocal white-light systems, all the wavelengths of light λ correspond to a common z-coordinate. The distance of the surface is coded by the peak position of the Gaussian-shaped depth response I(z). Thus, the measurement task is first to scan the depth response I(z) and second to determine the corresponding peak position.

A **c**hromatic **c**onfocal distance **p**robe (CCP) is not axially colour corrected [Molesini 1984]. On the contrary, the chromatic axial dispersion is maximized, whereas all the other optical aberrations were corrected [Jordan 2004]. Within a broadband wavelength range as given by the system design, different wavelengths were focused into different distances. This creates a continuous chromatic (wavelength) coding of the surface distance, as shown in Figure 2 and Figure 3.

The CCP's depth response I(λ) is also Gaussian-shaped. Thus, the measurement task in CCPs is first to grab the depth response I(λ) using a spectrometer equipped with a CCD line camera and second to determine the corresponding peak position. Contrary to monochromatic confocal distance measurement systems, CCPs are purely passive systems, they do not need a mechanical z-scan of the depth response.

Due to the continuous chromatic focus shift, the total envelope of the focus region (the so called "caustic") has a large "spot size", but this caustic's waste (which can be in the sub-millimetre range) is not the measurement spot size. On one side, the optical design of a CCP head is diffraction limited all over broadband wavelength range. On the other side, the focus spot size of a CCP head results from the size of the confocal pinhole as imaged by the CCP head itself. In practise, a CCP spot size is in the order of several microns.

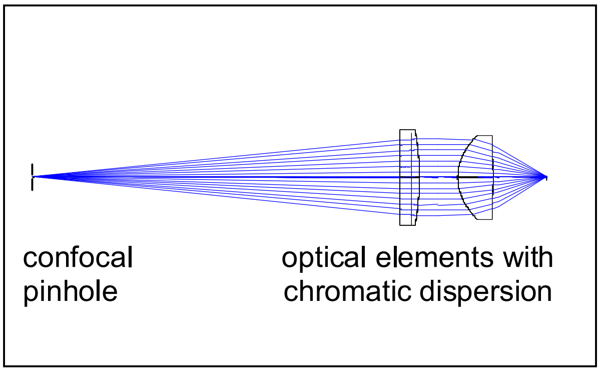

Figure 2: Schematic design of a CCP sensor head.

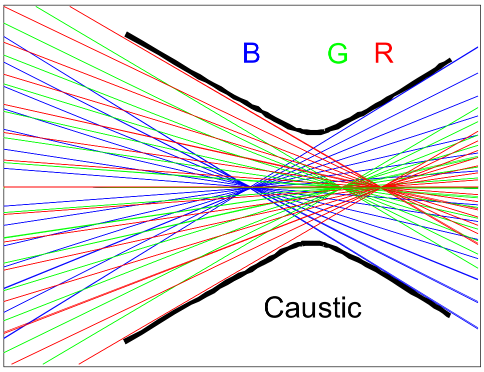

Figure 3: Focus zoom of Figure 2.

3. TECHNICAL DESIGN OF CHROMATIC CONFOCAL DISTANCE PROBES

The main components of a CCP system are a broadband white-light source, a spectrometer, a digital signal processor (DSP), a fiber coupler and the CCP sensor head. The complete optical scheme of a CCP system is shown in Figure 4. The external CCP sensor head as shown in Figure 2 is connected to the CCP controller, which contains all the other components, using a multimode fiber patch-cord of typically 50 µm core diameter, as shown in Figure 5. The head side fiber extremity acts both as the point light source as well as the pinhole.

A benefit of a CCP system is the scalability of the external CCP sensor head, due to its passive function. Scalable characteristic parameters of the CCP sensor head are measurement range, working distance, numerical aperture (NA) and to some extend other functionalities.

We have several CCP sensor heads with measurement ranges from 300 µm up to 4 mm [www.digitalsurf.de]. Figure 6 shows a 90 degree angled head with a measurement range of 400 µm, an average working distance of 5 mm, a numerical aperure of 0.5, a spot size of 5 µm, a repeatability of 20 nm and a linearity of ± 0,2 %.

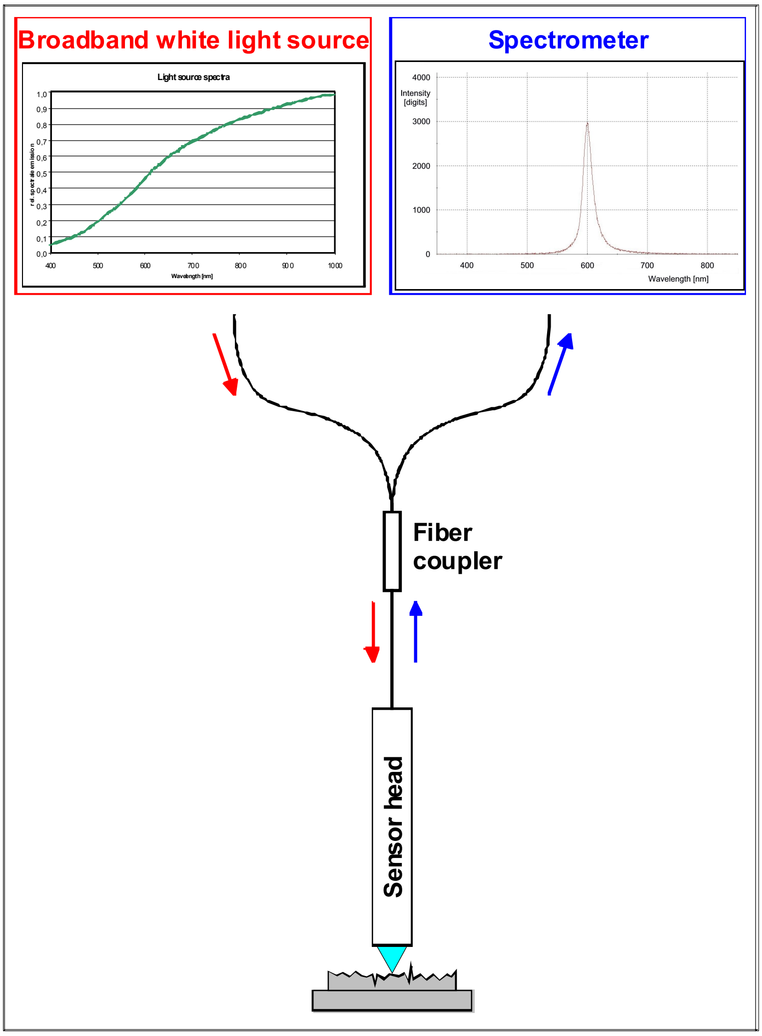

Figure 4: Optical scheme of a CCP system.

Figure 5: A CCP controller plus external CCP sensor head.

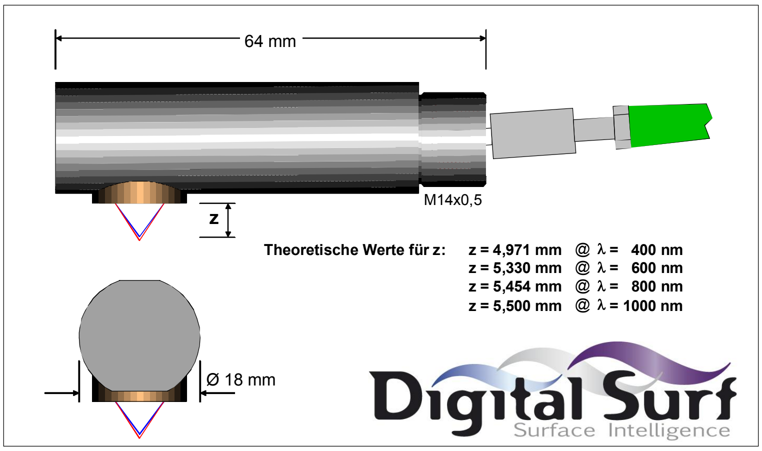

Figure 6: CCP sensor head RB-400 with 400 µm range.

4. THE PROBLEM OF SURFACE SLOPES

An important question in optical surface metrology is: What is the maximum surface slope angle that can be measured on tilted surfaces?

Figure 7 shows the corresponding geometry which is valid for all kinds of focusing techniques, not only for the CCP. A lens, completely been illuminated, is focusing the light under its aperture angle α. A smooth and mirror like surface element of slope angle β_S creates specular reflection under a beam deviation of $2\beta_S$ (index S for specular). As long as $\beta_S < \alpha$, a part of the reflected light is captured by the lens for detection.

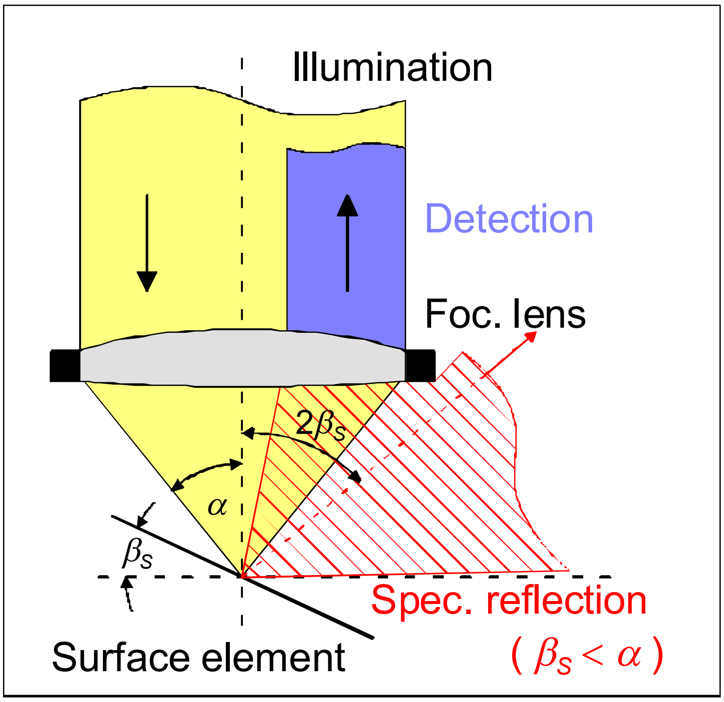

Figure 7: Specular reflection on surface slope angle $\beta_S < \alpha$.

The higher the numerical aperture (NA = sin α) of the focusing lens is, the higher the measurable maximum surface slope angle β_S can be in case of specular reflection. For $\beta_S \rightarrow \alpha$, the amount of detectable light decreases down to zero. Thus, the signal-to-noise-ratio SNR of the systems detector is also important. The higher the SNR is, the nearer β_S can converge towards α.

If the reflecting surface element is not smooth and mirror like but rough with some micro-roughness inside the measurement spot size, then the type of reflection changes from specular to diffuse, as shown in Figure 8. Diffuse reflection creates some scattering of light into a room angle which can exceed the aperture angle α dramatically. As a result of this, the macroscopic surface slope β_D (index D for diffuse) can also exceed the aperture angle α.

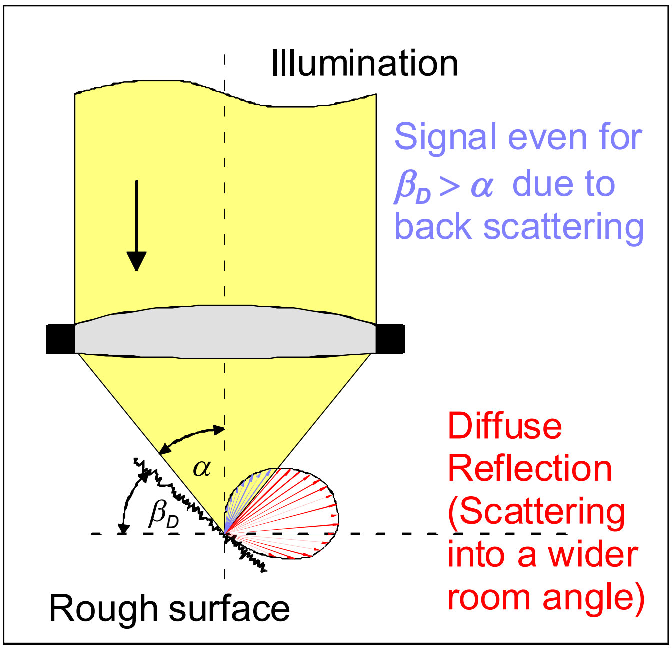

Figure 8: Diffuse reflection on macroscopic surface slope angle $\beta_D > \alpha$.

5. MEASUREMENT RESULTS

All images and data set operations within this section have been produced using our Digital Surf's MountainsMap software.

5.1 Slope analysis on form measurements

Figure 9 shows a 3D topography measurement of a piece of a Nylon thread of 1 mm diameter using an RB-1000 head with 1 mm range and 0.5 numerical aperture, which means a maximum slope angle for specular reflection of $\beta_{S,max}$ = 30 degree. Figure 10 shows a single raw data profile extracted from this 3D topography. In order to analyse the slope angles as shown in the profile of Figure 10, a circle has been fitted into the curved part of the raw data profile, as shown in Figure 11, together with 3 pairs of bars indicating some slope angles.

Figure 12 shows the difference between the raw data profile (Figure 10) and the fitted circle profile (Figure 11). The flat central plateau of this difference profile shows a good agreement of the measured and the expected surface slope angles. The right pair of bars in Figure 11 indicates the location of a surface slope of 30 degrees, which corresponds to the maximum surface slope angle $\beta_{S,max}$ of the RB-1000 head. Up to this slope angle, the corresponding part of the difference profile in Figure 12 is nearly perfectly flat. The centre pair of bars in Figure 11 indicates the location of a surface slope of 45 degrees. Between the slope angles of 30 and 45 degree, the corresponding part of the difference profile in Figure 12 remains on the same level but with some additional "noise", which indicates some small measurement errors. Finally, the left pair of bars in Figure 11 indicates the location of a surface slope of 75 degrees, which was about the limit before the CCP lost the signal due to exceeding surface slope angles. But even between 45 and 75 degrees, the raw data quality was acceptable.

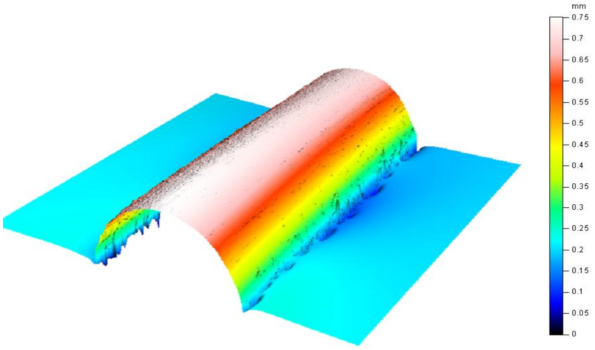

Figure 9: 3D topography of a Nylon thread of 1 mm diameter.

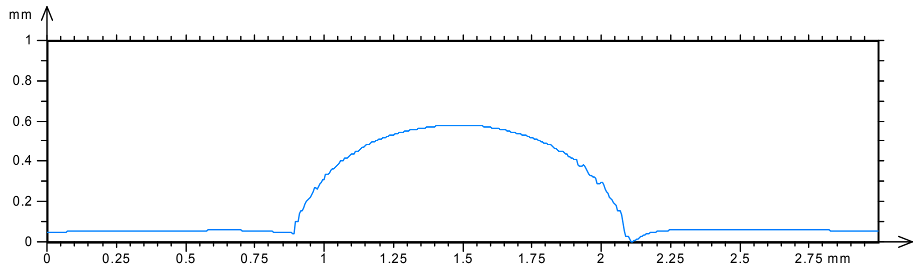

Figure 10: Raw data profile as extracted from the 3D topography in Figure 9.

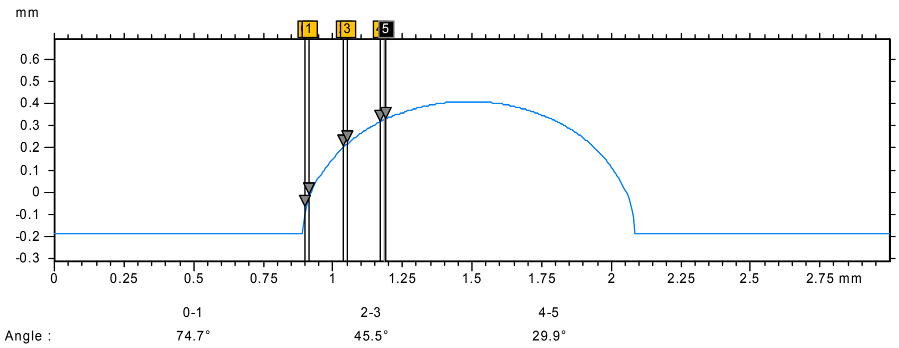

Figure 11: Part of a circle as fitted into the profile from Figure 10.

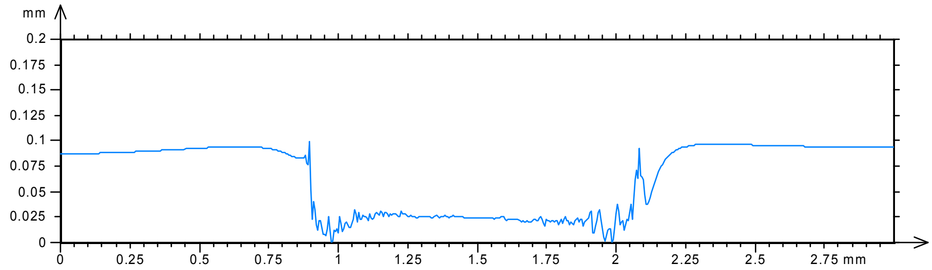

Figure 12: Difference between the raw data profile (Figure 10) and the fitted circle profile (Figure 11).

5.2 Thickness deviation analysis

Figure 13 shows a raw data 3D topography of the recycling logo from a drink dispenser's plastic cup. The contours of the logo are increased compared to the substrate. This measurement was taken from the inside bottom of the cup, using an RB-1000 head with 1 mm range and 0.5 numerical aperture.

Figure 14 shows the corresponding raw data 3D topography of the same logo, taken from the outside of the cup. Here, the contours of the logo are depressed compared to the substrate, due to the embossing fabrication process.

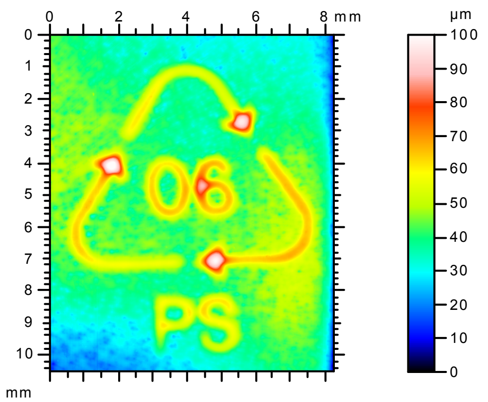

Figure 13: Raw data 3D topography of the inside recycling logo.

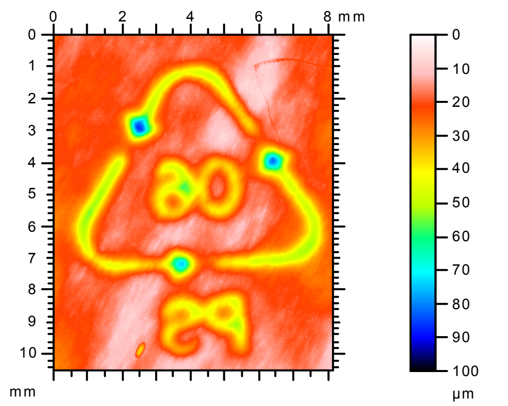

Figure 14: Raw data 3D topography of the outside recycling logo.

In order to analyse the thickness deviation of this 2 topographies, the topography as taken from the outside bottom of the cup (Figure 14) was first mirrored in the x direction and then inverted in height (z), as shown in Figure 15. As can be seen form Figure 15, the contours from the outside bottom of the cup appear less sharp than the contours from the inside bottom of the cup (Figure 13). In addition, the logo contours form the topographies from Figure 13 and Figure 15 show some lateral as well as rotational shift with respect to each other. Rotating the topography from Figure 15 by 4 degrees and applying the "surface subtraction" operation to the resulting rotated topography as well as to the topography from Figure 13 creates the topographies from Figures 16 and 17, which now show the best coincidence in the logo's contours. These two Figures 16 and 17 also show some interesting differences in the substrate's fine structure.

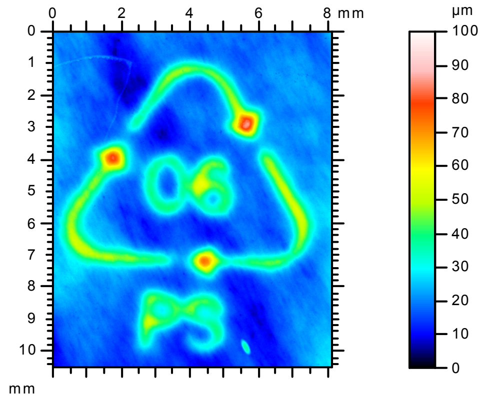

Figure 15: Topography from Figure 14, mirrored in x and inverted in z.

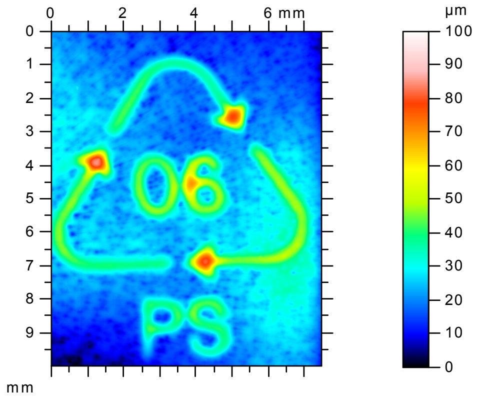

Figure 16: Topography from Figure 13, after the “surface subtraction”.

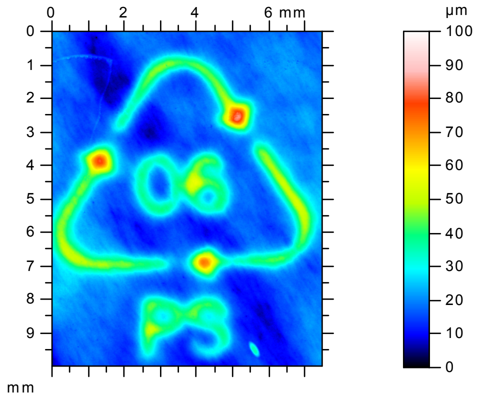

Figure 17: Topography from Figure 15, after 1st a 4 degree rotation and 2nd the “surface subtraction”.

The resulting thickness deviation topography in Figure 18 was obtained by subtracting both the topographies from Figures 16 and 17.

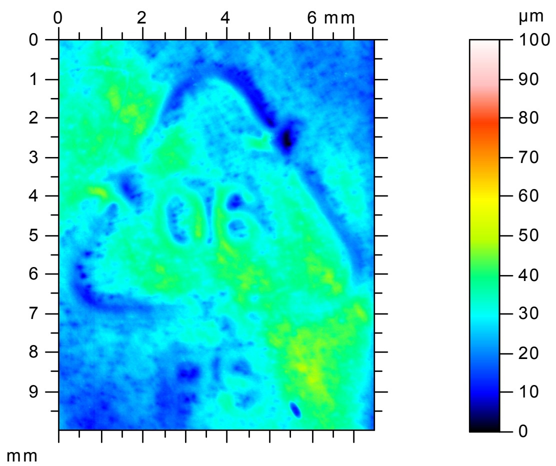

Figure 18: Thickness deviation topography.

6. REFERENCES

[Carlsson 1987] Carlsson K. and Åslund N; “Confocal imaging for 3-D digital microscopy”; In: *Appl. Opt. 26 No 16*, (1987), pp. 3232

[Hamilton 1981] Hamilton D. K., Wilson T., and Sheppard C. J. R.; “Experimental observation of the depth-discrimination properties of scanning microscopes”; In: *Opt. Lett. 6 No 12*, (1981), pp. 625

[Hamilton 1982] Hamilton D. K. and Wilson T.; “Three-dimensional Surface Measurement using the confocal scanning microscope”; In: *Appl. Phys. B 27*, (1982), pp. 211

[Jordan 1997] Jordan H.-J., Wegner M., and Tiziani H.; “Optical topometry for roughness measurement and form analysis of engineering surfaces using confocal microscopy”; In: *Progress in Precision Engineering and Nanotechnolgy, Proceedings of the 9th International Precision Engineering Seminar / 4th International Conference on Ultraprecision in Manufacturing Engineering*, (1997), pp. 171; ISBN 3-9801433-9-2

[Jordan 1998] Jordan H.-J., Wegner M., and Tiziani H.; “Highly accurate non-contact characterisation of engineering surfaces using confocal microscopy”; In: *Meas. Sci. Technol. 9*, (1998), pp. 1142

[Jordan 2000] Jordan H.-J., Brodmann R.; “Highly accurate surface measurement by means of white light confocal microscopy”; In: *X. International Colloquium on Surfaces, Chemnitz University of Technology*, (2000), pp. 296

[Jordan 2001] Jordan, H.-J., et al.; „Quality assurance of HARMS and MOEMS surface structures using confocal white light microscopy“, In: *SPIE Proceedings 4400*, (2001), pp. 51-58

[Jordan 2004] Jordan, H.-J.; “Highly accurate 2D and 3D surface metrology using confocal white-light sensors with chromatic distance coding”; In: *XI. International Colloquium on Surfaces, Chemnitz University of Technology*, (2004), pp. 127

[Minsky 1957] Minsky M.; "Microscopy Apparatus"; In: *U.S. Patent 3013467* (19 Dec. 1961, filed 7 November 1957)

[Minsky 1988] Minsky M.; "Memoir on Inventing the Confocal Scanning Microscope"; In: *Scanning 10 No 4*, (1988), pp. 128

[Molesini 1984] Molesini G., Pedrini G., Poggi P., and Quercioli F.; “Focus-wavelength encoded optical profilometer”; In: *Optics Comm. 49 No 4*, (1984), pp. 229

[Petran 1968] Petran M., Hadravsky M., Egger M. D. and Galambos R.; “Tandem-Scanning Reflected-Light Microscope”; In: *J. Opt. Soc. Am. 58 No 5*, (1968), pp. 661

[Wilson 1989] Wilson T.; "Depth response of scanning microscopes"; In: *Optik 81 No 3*, (1989), pp. 113

[Wilson 1990] Wilson T.; “Confocal Microscopy”; Academic Press, (1990)